Hindawi
Complexity
Volume 2019, Article ID 7408725, 16 pages
https://doi.org/10.1155/2019/7408725

Research Article

End-Point Static Control of Basic Oxygen Furnace (BOF) Steelmaking Based on Wavelet Transform Weighted Twin Support Vector Regression

Chuang Gao,[1,2] Minggang Shen ,[1] Xiaoping Liu,[3] Lidong Wang,[2] and Maoxiang Chu[2]

[1]*School of Materials and Metallurgy, University of Science and Technology Liaoning, Anshan, Liaoning, China*
[2]*School of Electronic and Information Engineering, University of Science and Technology Liaoning, Anshan, Liaoning, China*
[3]*School of Information and Electrical Engineering, Shandong Jianzhu University, Jinan, Shandong, China*

Correspondence should be addressed to Minggang Shen; lnassmg@163.com

Received 6 July 2018; Revised 22 October 2018; Accepted 10 December 2018; Published 1 January 2019

Academic Editor: Michele Scarpiniti

A static control model is proposed based on wavelet transform weighted twin support vector regression (WTWTSVR). Firstly, new weighted matrix and coefficient vector are added into the objective functions of twin support vector regression (TSVR) to improve the performance of the algorithm. The performance test confirms the effectiveness of WTWTSVR. Secondly, the static control model is established based on WTWTSVR and 220 samples in real plant, which consists of prediction models, control models, regulating units, controller, and BOF. Finally, the results of proposed prediction models show that the prediction error bound with 0.005% in carbon content and 10°C in temperature can achieve a hit rate of 92% and 96%, respectively. In addition, the double hit rate of 90% is the best result by comparing with four existing methods. The results of the proposed static control model indicate that the control error bound with 800 Nm^3 in the oxygen blowing volume and 5.5 *tons* in the weight of auxiliary materials can achieve a hit rate of 90% and 88%, respectively. Therefore, the proposed model can provide a significant reference for real BOF applications, and also it can be extended to the prediction and control of other industry applications.

1. Introduction

With the development of end-point control technology for basic oxygen furnace (BOF), the static control model can be established to overcome the randomness and inconsistency of the artificial experience control models. According to the initial conditions of hot metal, the relative calculations can be carried out to guide production. The end-point hit rate would be improved through this approach. Unfortunately, the control parameters would not be adjusted during the smelting process, which restricts the further improvement of the end-point hit rate. To solve this problem, the sublance based dynamic control model could be adopted by using the sublance technology. By combining the static model with the dynamic model, the end-point hit rate of BOF could be guaranteed. The establishment of the static control model is the foundation of the dynamic model. The accuracy of the static model will directly affect the hit rates of the dynamic control model, thus it plays an important role in the parameter optimization of BOF control process. Therefore, the static control model is still a practical and reliable technology to guide the production and improve the technology and management level of steelmaking plants.

In recent years, some significant developments of BOF prediction and control modelling have been achieved. Blanco et al. [1] designed a mixed controller for carbon and silicon in a steel converter in 1993. In 2002, three back propagation models are adopted to predict the end-blow oxygen volume and the weight of coolant additions [2]. In 2006, a dynamic model is constructed to predict the carbon content and temperature for the end-blow stage of BOF [3]. Based on multivariate data analysis, the slopping prediction was proposed by Brämming et al. [4]. In 2014, the multi-level recursive regression model was established for the prediction of end-point phosphorus content during BOF steelmaking process [5]. An antijamming endpoint prediction model

of extreme learning machine (ELM) was proposed with evolving membrane algorithm [6]. By applying input variables selection technique, the input weighted support vector machine modelling was proposed [7], and then the prediction model was established on the basis of improving a case-based reasoning method [8]. The neural network prediction modellings [9–12] were carried out to achieve aimed end-point conditions in liquid steel. A fuzzy logic control scheme was given for the basic oxygen furnace in [13]. Most of these achievements are based on the statistical and intelligent methods.

As an intelligent method, Jayadeva et. al. [14] proposed a twin support vector machine (TSVM) algorithm in 2007. The advantage of this method is that the computational complexity of modelling can be reduced by solving two quadratic programming problems instead of one in traditional method. It is also widely applied to the classification applications. In 2010, Peng [15] proposed a twin support vector regression (TSVR), which can be used to establish the prediction model for industrial data. After that, some improved TSVR methods [16–22] were proposed. By introducing a K-nearest neighbor (KNN) weighted matrix into the optimization problem in TSVR, the modified algorithms [16, 19] were proposed to improve the performance of TSVR. A v-TSVR [17] and asymmetric v-TSVR [20] were proposed to enhance the generalization ability by tuning new model parameters. To solve the ill-conditioned problem in the dual objective functions of the traditional TSVR, an implicit Lagrangian formulation for TSVR [18] was proposed to ensure that the matrices in the formulation are always positive semidefinite matrices. Parastalooi et al. [21] added a new term into the objective function to obtain structural information of the input data. By comparing with the neural network technology, the disadvantage of neural network is that the optimization process may fall into the local optimum. The optimization of TSVR is a pair of quadratic programming problems (QPPs), which means there must be a global optimal solution for each QPP. All above modified TSVR algorithms are focused on the improvements of the algorithm accuracy and the computation speed. Currently, the TSVR algorithm has never been adopted in the BOF applications. Motivated by this, the TSVR algorithm can be used to establish a BOF model.

Wavelet transform can fully highlight the characteristics of some aspects of the problem, which has attracted more and more attention and been applied to many engineering fields. In this paper, the wavelet transform technique is used to denoise the output samples during the learning process, and it is a new application of the combination of wavelet transform and support vector machine method. Then, a novel static control model is proposed based on wavelet transform weighted twin support vector regression (WTWTSVR), which is an extended model of our previous work. In [23], we proposed an end-point prediction model with WTWTSVR for the carbon content and temperature of BOF, and the accuracy of the prediction model is expected. However, the prediction model cannot be used to guide real BOF production directly. Hence, a static control model should be established based on the prediction model to calculate the oxygen volume and the weight of auxiliary raw materials, and the accuracy of the calculations affects the quality of the steel. Therefore, the proposed control model can provide a guiding significance for real BOF production. It is also helpful to other metallurgical prediction and control applications. To improve the performance of the control model, an improvement of the traditional TSVR algorithm is carried out. A new weighted matrix and a coefficient vector are added into the objective function of TSVR. Also, the parameter ε in TSVR is not adjustable anymore, which means it is a parameter to be optimized. Finally, the static control model is established based on the real datasets collected from the plant. The performance of the proposed method is verified by comparing with other four existing regression methods. The contributions of this work include the following. (1) It is the first attempt to establish the static control model of BOF by using the proposed WTWTSVR algorithm. (2) New weighted matrix and coefficient vector are determined by the wavelet transform theory, which gives a new idea for the optimization problem in TSVR areas. (3) The proposed algorithm is an extension of the TSVR algorithm, which is more flexible and accurate to establish a prediction and control model. (4) The proposed control model provides a new approach for the applications of BOF control. The application range of the proposed method could be extended to other metallurgical industries such as the prediction and control in the blast furnace process and continuous casting process.

Remark 1. The main difference between primal KNNWTSVR [16] and the proposed method is that the proposed algorithm utilizes the wavelet weighted matrix instead of KNN weighted matrix for the squared Euclidean distances from the estimated function to the training points. Also, a wavelet weighted vector is introduced into the objective functions for the slack vectors. ε_1 and ε_2 are taken as the optimized parameters in the proposed algorithm to enhance the generalization ability. Another difference is that the optimization problems of the proposed algorithm are solved in the Lagrangian dual space and that of KNNWTSVR are solved in the primal space via unconstrained convex minimization.

Remark 2. By comparing with available weighted technique like K-nearest neighbor, the advantages of the wavelet transform weighting scheme are embodied in the following two aspects:

(1) The Adaptability of the Samples. The proposed method is suitable for dealing with time/spatial sequence samples (such as the samples adopted in this paper) due to the character of wavelet transform. The wavelet transform inherits and develops the idea of short-time Fourier transform. The weights of sample points used in the proposed algorithm are determined by calculating the difference between the sample values and the wavelet-regression values for Gaussian function, which can mitigate the noise, especially the influence of outliers. While KNN algorithm determines the weight of the sample points by calculating the number of adjacent points (determined by Euclidian distance), which is more suitable for the samples of multi-points clustering type distribution.

(2) The Computational Complexity. KNN algorithm requires a large amount of computations, because the distance between each sample to all known samples must be computed to obtain its K nearest neighbors. By comparing with KNN weighting scheme, the wavelet transform weighting scheme has less computational complexity, because it is dealing with one dimensional output samples, and the computation complexity is proportional to the number of samples l. KNN scheme is dealing with the input samples, the computation complexity of KNN scheme is proportional to l^2. With the increasing of dimensions and number of the samples, it will have a large amount of computations.

Therefore, the wavelet transform weighting scheme is more competitive than KNN weighting scheme for the time sequence samples due to its low computational complexity.

2. Background

2.1. Description of BOF Steelmaking. BOF is used to produce the steel with wide range of carbon, alloy, and special alloy steels. Normally, the capacity of BOF is between 100 *tons* and 400 *tons*. When the molten iron is delivered to the converter through the rail, the desulphurization process is firstly required. In BOF, the hot metal and scrap, lime, and other fluxes are poured into the converter. The oxidation reaction is carried out with carbon, silicon, phosphorus, manganese, and some iron by blowing in a certain volume of oxygen. The ultimate goal of steelmaking is to produce the steel with specific chemical composition at suitable tapping temperature. The control of BOF is difficult because the whole smelting process is only half an hour, and there is no opportunity for sampling and analysis in the smelting process. The proportion of the iron and scrap is about 3:1 in BOF. The crane loads the waste into the container and then pours the molten iron into the converter. The water cooled oxygen lance enters the converter, the high purity oxygen is blown into BOF at 16000 cubic feet per minute, and the oxygen is reacted with carbon and other elements to reduce the impurity in the molten metal and converts it into a clean, high quality liquid steel. The molten steel is poured into the ladle and sent to the metallurgical equipment of the ladle [13].

Through the oxidation reaction of oxygen blown in BOF, the molten pig iron and the scrap can be converted into steel. It is a widely used steelmaking method with its higher productivity and low production cost [3]. However, the physical and chemical process of BOF is very complicated. Also, there are various types of steel produced in the same BOF, which means that the grade of steel is changed frequently. Therefore, the BOF modelling is a challenge task. The main objective of the modelling is to obtain the prescribed end-point carbon content and temperature.

2.2. Nonlinear Twin Support Vector Regression. Support vector regression (SVR) was proposed for the applications of regression problems. For the nonlinear case, it is based on the structural risk minimization and Vapnik ε-insensitive loss function. In order to improve the training speed of SVR, Peng proposed a TSVR algorithm in 2010. The difference between TSVR and SVR is that SVR solves one large QPP problem and TSVR solves two small QPP problems to improve the learning efficiency. Assume that a sample is an n-dimensional vector and the number of the samples is l, which can be expressed as $(\mathbf{x}_1, y_1), \ldots, (\mathbf{x}_l, y_l)$. Let $\mathbf{A} = [\mathbf{x}_1, \ldots, \mathbf{x}_l]^T \in R^{l\times n}$ be the input data set of training samples, $\mathbf{y} = [y_1, \ldots, \mathrm{y}_l]^T \in R^l$ be the corresponding output, and $\mathbf{e} = [1, \ldots, 1]^T$ be the ones vector with appropriate dimensions. Assume $K(.,.)$ denotes a nonlinear kernel function. Let $K(\mathbf{A}, \mathbf{A}^T)$ be the kernel matrix with order l and its (i, j)-th element $(i, j = 1, 2, \ldots, l)$ be defined by

$$\left[K\left(\mathbf{A}, \mathbf{A}^T\right)\right]_{i,j} = K\left(\mathbf{x}_i, \mathbf{x}_j\right) = \left(\Phi\left(\mathbf{x}_i\right) \cdot \Phi\left(\mathbf{x}_j\right)\right) \in R. \quad (1)$$

Here, the kernel function $K(\mathbf{x}, \mathbf{x}_i)$ represents the inner product of the nonlinear mapping functions $\Phi(\mathbf{x}_i)$ and $\Phi(\mathbf{x}_j)$ in the high dimensional feature space. Because there are various kernel functions, the performance comparisons of kernel functions will be discussed later. In this paper, the radial basis kernel function (RBF) is chosen as follows:

$$K\left(\mathbf{x}, \mathbf{x}_i\right) = \exp\left(-\frac{\left\|\mathbf{x} - \mathbf{x}_i\right\|^2}{2\sigma^2}\right), \quad (2)$$

where σ is the width of the kernel function. Let $K(\mathbf{x}^T, \mathbf{A}^T) = (K(\mathbf{x}, \mathbf{x}_1), K(\mathbf{x}, \mathbf{x}_2), \ldots, K(\mathbf{x}, \mathbf{x}_l))$ be a row vector in R^l. Then, two ε-insensitive bound functions $f_1(\mathbf{x}) = K(\mathbf{x}^T, \mathbf{A}^T)\boldsymbol{\omega}_1 + b_1$ and $f_2(\mathbf{x}) = K(\mathbf{x}^T, \mathbf{A}^T)\boldsymbol{\omega}_2 + b_2$ can be obtained, where $\boldsymbol{\omega}_1, \boldsymbol{\omega}_2 \in R^l$ are the normal vectors and $b_1, b_2 \in R$ are the bias values. Therefore, the final regression function $f(\mathbf{x})$ is determined by the mean of $f_1(\mathbf{x})$ and $f_2(\mathbf{x})$, that is,

$$\begin{aligned} f\left(\mathbf{x}\right) &= \frac{1}{2}\left(f_1\left(\mathbf{x}\right) + f_2\left(\mathbf{x}\right)\right) \\ &= \frac{1}{2}K\left(\mathbf{x}^T, \mathbf{A}^T\right)\left(\boldsymbol{\omega}_1 + \boldsymbol{\omega}_2\right) + \frac{1}{2}\left(b_1 + b_2\right). \end{aligned} \quad (3)$$

Nonlinear TSVR can be obtained by solving two QPPs as follows:

$$\begin{aligned} \min_{\boldsymbol{\omega}_1, b_1, \boldsymbol{\xi}} \quad & \frac{1}{2}\left\|\mathbf{y} - \varepsilon_1\mathbf{e} - \left(K\left(\mathbf{A}, \mathbf{A}^T\right)\boldsymbol{\omega}_1 + b_1\mathbf{e}\right)\right\|^2 + c_1\mathbf{e}^T\boldsymbol{\xi} \\ \text{s.t.:} \quad & \mathbf{y} - \left(K\left(\mathbf{A}, \mathbf{A}^T\right)\boldsymbol{\omega}_1 + b_1\mathbf{e}\right) \geq \varepsilon_1\mathbf{e} - \boldsymbol{\xi}, \quad \boldsymbol{\xi} \geq 0e, \end{aligned} \quad (4)$$

and

$$\begin{aligned} \min_{\boldsymbol{\omega}_2, b_2, \boldsymbol{\gamma}} \quad & \frac{1}{2}\left\|\mathbf{y} + \varepsilon_2\mathbf{e} - \left(K\left(\mathbf{A}, \mathbf{A}^T\right)\boldsymbol{\omega}_2 + b_2\mathbf{e}\right)\right\|^2 + c_2\mathbf{e}^T\boldsymbol{\gamma} \\ \text{s.t.:} \quad & K\left(\mathbf{A}, \mathbf{A}^T\right)\boldsymbol{\omega}_2 + b_2\mathbf{e} - \mathbf{y} \geq \varepsilon_2\mathbf{e} - \boldsymbol{\gamma}, \quad \boldsymbol{\gamma} \geq 0\mathbf{e}, \end{aligned} \quad (5)$$

By introducing the Lagrangian function and Karush-Kuhn-Tucker conditions, the dual formulations of (4) and (5) can be derived as follows:

$$\begin{aligned} \max_{\boldsymbol{\alpha}} \quad & -\frac{1}{2}\boldsymbol{\alpha}^T\mathbf{G}\left(\mathbf{G}^T\mathbf{G}\right)^{-1}\mathbf{G}^T\boldsymbol{\alpha} + \mathbf{g}^T\mathbf{G}\left(\mathbf{G}^T\mathbf{G}\right)^{-1}\mathbf{G}^T\boldsymbol{\alpha} \\ & - \mathbf{g}^T\boldsymbol{\alpha} \\ \text{s.t.:} \quad & 0\mathbf{e} \leq \boldsymbol{\alpha} \leq c_1\mathbf{e}, \end{aligned} \quad (6)$$

and

$$\begin{aligned}\max_{\boldsymbol{\beta}} \quad & -\frac{1}{2}\boldsymbol{\beta}^T\mathbf{G}\left(\mathbf{G}^T\mathbf{G}\right)^{-1}\mathbf{G}^T\boldsymbol{\beta} - \mathbf{h}^T\mathbf{G}\left(\mathbf{G}^T\mathbf{G}\right)^{-1}\mathbf{G}^T\boldsymbol{\beta} \\ & + \mathbf{h}^T\boldsymbol{\beta} \\ \text{s.t.:} \quad & 0\mathbf{e} \le \boldsymbol{\beta} \le c_2\mathbf{e},\end{aligned} \tag{7}$$

where $\mathbf{G} = [K(\mathbf{A}, \mathbf{A}^T), \mathbf{e}]$, $\mathbf{g} = \mathbf{y} - \varepsilon_1\mathbf{e}$, and $\mathbf{h} = \mathbf{y} + \varepsilon_2\mathbf{e}$.

To solve the above QPPs (6) and (7), the vectors $\boldsymbol{\omega}_1, b_1$ and $\boldsymbol{\omega}_2, b_2$ can be obtained:

$$\begin{bmatrix}\boldsymbol{\omega}_1 \\ b_1\end{bmatrix} = \left(\mathbf{G}^T\mathbf{G}\right)^{-1}\mathbf{G}^T\left(\mathbf{g} - \boldsymbol{\alpha}\right), \tag{8}$$

and

$$\begin{bmatrix}\boldsymbol{\omega}_2 \\ b_2\end{bmatrix} = \left(\mathbf{G}^T\mathbf{G}\right)^{-1}\mathbf{G}^T\left(\mathbf{h} + \boldsymbol{\beta}\right). \tag{9}$$

By substituting the above results into (3), the final regression function can be obtained.

2.3. Nonlinear Wavelet Transform Based Weighted Twin Support Vector Regression

2.3.1. Model Description of Nonlinear WTWTSVR. In 2017, Xu el. al. [20] proposed the asymmetric ν-TSVR algorithm based on pinball loss functions. This new algorithm can enhance the generalization ability by tuning new model parameters. The QPPs of nonlinear asymmetric ν-TSVR were proposed as follows:

$$\begin{aligned}\min_{\boldsymbol{\omega}_1, b_1, \boldsymbol{\xi}, \varepsilon_1} \quad & \frac{1}{2}\left\|\mathbf{y} - \left(K\left(\mathbf{A}, \mathbf{A}^T\right)\boldsymbol{\omega}_1 + b_1\mathbf{e}\right)\right\|^2 + c_1\nu_1\varepsilon_1 \\ & + \frac{1}{l}c_1\mathbf{e}^T\boldsymbol{\xi} \\ \text{s.t.:} \quad & \mathbf{y} - \left(K\left(\mathbf{A}, \mathbf{A}^T\right)\boldsymbol{\omega}_1 + b_1\mathbf{e}\right) \\ & \ge -\varepsilon_1\mathbf{e} - 2\left(1 - p\right)\boldsymbol{\xi}, \quad \boldsymbol{\xi} \ge 0\mathbf{e}, \ \varepsilon_1 \ge 0\end{aligned} \tag{10}$$

and

$$\begin{aligned}\min_{\boldsymbol{\omega}_2, b_2, \varepsilon_2, \boldsymbol{\gamma}} \quad & \frac{1}{2}\left\|\mathbf{y} - \left(K\left(\mathbf{A}, \mathbf{A}^T\right)\boldsymbol{\omega}_2 + b_2\mathbf{e}\right)\right\|^2 + c_2\nu_2\varepsilon_2 \\ & + \frac{1}{l}c_2\mathbf{e}^T\boldsymbol{\xi}^* \\ \text{s.t.:} \quad & K\left(\mathbf{A}, \mathbf{A}^T\right)\boldsymbol{\omega}_2 + b_2\mathbf{e} - \mathbf{y} \ge -\varepsilon_2\mathbf{e} - 2p\boldsymbol{\xi}^*, \\ & \boldsymbol{\xi}^* \ge 0\mathbf{e}, \ \varepsilon_2 \ge 0\end{aligned} \tag{11}$$

where $c_1, c_2, \nu_1, \nu_2 \ge 0$ are regulating parameters and the parameter $p \in (0, 1)$ is used to apply a slightly different penalty for the outliers. The contributions of this method are that ε_1 and ε_2 are introduced into the objective functions of QPPs, and the parameters ν_1 and ν_2 are used to regulate the width of ε_1 and ε_2 tubes. Also, the parameter p is designed to give an unbalance weight for the slack vectors $\boldsymbol{\xi}$ and $\boldsymbol{\xi}^*$. Based on the concept of asymmetric ν-TSVR, a nonlinear wavelets transform based weighted TSVR is firstly proposed in this paper. By comparing with the traditional TSVR algorithm, the proposed algorithm introduces a wavelet transform based weighted matrix $\mathbf{D}_1$ and a coefficient vector $\mathbf{D}_2$ into the objective function of TSVR. Also, the parameters ε_1 and ε_2 are not adjustable by user anymore, which means they are both introduced into the objective functions. Simultaneously, the regularization is also considered to obtain the optimal solutions. Therefore, the QPPs of nonlinear WTWTSVR are proposed as follows:

$$\begin{aligned}\min_{\boldsymbol{\omega}_1, b_1, \boldsymbol{\xi}, \varepsilon_1} \quad & \frac{1}{2}\left(\mathbf{y} - \left(K\left(\mathbf{A}, \mathbf{A}^T\right)\boldsymbol{\omega}_1 + b_1\mathbf{e}\right)\right)^T\mathbf{D}_1\left(\mathbf{y} - \left(K\left(\mathbf{A}, \mathbf{A}^T\right)\boldsymbol{\omega}_1 + b_1\mathbf{e}\right)\right) + \frac{c_1}{2}\left(\boldsymbol{\omega}_1^T\boldsymbol{\omega}_1 + b_1^2\right) + c_2\left(\mathbf{D}_2^T\boldsymbol{\xi} + \nu_1\varepsilon_1\right) \\ \text{s.t.:} \quad & \mathbf{y} - \left(K\left(\mathbf{A}, \mathbf{A}^T\right)\boldsymbol{\omega}_1 + b_1\mathbf{e}\right) \ge -\varepsilon_1\mathbf{e} - \boldsymbol{\xi}, \quad \boldsymbol{\xi} \ge 0\mathbf{e}, \ \varepsilon_1 \ge 0,\end{aligned} \tag{12}$$

and

$$\begin{aligned}\min_{\boldsymbol{\omega}_2, b_2, \boldsymbol{\xi}^*, \varepsilon_2} \quad & \frac{1}{2}\left(\mathbf{y} - \left(K\left(\mathbf{A}, \mathbf{A}^T\right)\boldsymbol{\omega}_2 + b_2\mathbf{e}\right)\right)^T\mathbf{D}_1\left(\mathbf{y} - \left(K\left(\mathbf{A}, \mathbf{A}^T\right)\boldsymbol{\omega}_2 + b_2\mathbf{e}\right)\right) + \frac{c_3}{2}\left(\boldsymbol{\omega}_2^T\boldsymbol{\omega}_2 + b_1^2\right) + c_4\left(\mathbf{D}_2^T\boldsymbol{\xi}^* + \nu_2\varepsilon_2\right) \\ \text{s.t.:} \quad & K\left(\mathbf{A}, \mathbf{A}^T\right)\boldsymbol{\omega}_2 + b_2\mathbf{e} - \mathbf{y} \ge -\varepsilon_2\mathbf{e} - \boldsymbol{\xi}^*, \quad \boldsymbol{\xi}^* \ge 0\mathbf{e}, \ \varepsilon_2 \ge 0,\end{aligned} \tag{13}$$

where $c_1, c_2, c_3, c_4, \nu_1, \nu_2 \ge 0$ are regulating parameters, $\mathbf{D}_1$ is a diagonal matrix with the order of $l \times l$, and $\mathbf{D}_2$ is a coefficient vector with the length of $l \times 1$. The determination of $\mathbf{D}_1$ and $\mathbf{D}_2$ will be discussed later.

The first term in the objective function of (12) or (13) is used to minimize the sums of squared Euclidean distances from the estimated function $f_1(\mathbf{x}) = K(\mathbf{x}^T, \mathbf{A}^T)\boldsymbol{\omega}_1 + b_1$ or $f_2(\mathbf{x}) = K(\mathbf{x}^T, \mathbf{A}^T)\boldsymbol{\omega}_2 + b_2$ to the training points. The matrix $\mathbf{D}_1$ gives different weights for each Euclidean distance. The second term is the regularization term to avoid the overfitting problem. The third term minimizes the slack vector $\boldsymbol{\xi}$ or $\boldsymbol{\xi}^*$ and the width of ε_1-tube or ε_2-tube. The coefficient vector $\mathbf{D}_2$ is a penalty vector for the slack vector. To solve the problem in (12), the Lagrangian function can be introduced, that is,

$$\begin{aligned} &L(\boldsymbol{\omega}_1, b_1, \boldsymbol{\xi}, \varepsilon_1, \boldsymbol{\alpha}, \boldsymbol{\beta}, \gamma) \\ &= \frac{1}{2}\left(\mathbf{y} - \left(K\left(\mathbf{A}, \mathbf{A}^T\right)\boldsymbol{\omega}_1 + b_1\mathbf{e}\right)\right)^T \\ &\cdot \mathbf{D}_1\left(\mathbf{y} - \left(K\left(\mathbf{A}, \mathbf{A}^T\right)\boldsymbol{\omega}_1 + b_1\mathbf{e}\right)\right) \\ &+ \frac{c_1}{2}\left(\boldsymbol{\omega}_1^T\boldsymbol{\omega}_1 + b_1^2\right) + c_2\left(\mathbf{D}_2^T\boldsymbol{\xi} + \nu_1\varepsilon_1\right) \\ &- \boldsymbol{\alpha}^T\left(\mathbf{y} - \left(K\left(\mathbf{A}, \mathbf{A}^T\right)\boldsymbol{\omega}_1 + b_1\mathbf{e}\right) + \varepsilon_1\mathbf{e} + \boldsymbol{\xi}\right) - \boldsymbol{\beta}^T\boldsymbol{\xi} \\ &- \gamma\varepsilon_1, \end{aligned} \tag{14}$$

where $\boldsymbol{\alpha}$, $\boldsymbol{\beta}$, and γ are the positive Lagrangian multipliers. By differentiating L with respect to the variables $\boldsymbol{\omega}_1, b_1, \boldsymbol{\xi}, \varepsilon_1$, we have

$$\begin{aligned} \frac{\partial L}{\partial \boldsymbol{\omega}_1} &= -K\left(\mathbf{A}, \mathbf{A}^T\right)^T\mathbf{D}_1\left(\mathbf{y} - \left(K\left(\mathbf{A}, \mathbf{A}^T\right)\boldsymbol{\omega}_1 + b_1\mathbf{e}\right)\right) \\ &\quad + K\left(\mathbf{A}, \mathbf{A}^T\right)^T\boldsymbol{\alpha} + c_1\boldsymbol{\omega}_1 = 0, \end{aligned} \tag{15}$$

$$\begin{aligned} \frac{\partial L}{\partial b_1} &= -\mathbf{e}^T\mathbf{D}_1\left(\mathbf{y} - \left(K\left(\mathbf{A}, \mathbf{A}^T\right)\boldsymbol{\omega}_1 + b_1\mathbf{e}\right)\right) + \mathbf{e}^T\boldsymbol{\alpha} \\ &\quad + c_1 b_1 = 0, \end{aligned} \tag{16}$$

$$\frac{\partial L}{\partial \boldsymbol{\xi}} = c_2\mathbf{D}_2 - \boldsymbol{\alpha} - \boldsymbol{\beta} = 0, \tag{17}$$

$$\frac{\partial L}{\partial \varepsilon_1} = c_2\nu_1 - \mathbf{e}^T\boldsymbol{\alpha} - \gamma = 0, \tag{18}$$

The K.K.T. conditions are given by

$$\begin{aligned} \mathbf{y} - \left(K\left(\mathbf{A}, \mathbf{A}^T\right)\boldsymbol{\omega}_1 + b_1\mathbf{e}\right) &\geq -\varepsilon_1\mathbf{e} - \boldsymbol{\xi}, \\ \boldsymbol{\xi} &\geq 0\mathbf{e}, \\ \boldsymbol{\alpha}^T\left(\mathbf{y} - \left(K\left(\mathbf{A}, \mathbf{A}^T\right)\boldsymbol{\omega}_1 + b_1\mathbf{e}\right) + \varepsilon_1\mathbf{e} + \boldsymbol{\xi}\right) &= 0, \\ \boldsymbol{\alpha} &\geq 0\mathbf{e}, \\ \boldsymbol{\beta}^T\boldsymbol{\xi} &= 0, \\ \boldsymbol{\beta} &\geq 0\mathbf{e}, \\ \gamma\varepsilon_1 = 0, \quad \gamma &\geq 0. \end{aligned} \tag{19}$$

Combining (15) and (16), we obtain

$$\begin{aligned} &-\begin{bmatrix} K\left(\mathbf{A}, \mathbf{A}^T\right)^T \\ \mathbf{e}^T \end{bmatrix}\mathbf{D}_1\left(\mathbf{y} - \left(K\left(\mathbf{A}, \mathbf{A}^T\right)\boldsymbol{\omega}_1 + b_1\mathbf{e}\right)\right) \\ &+ \begin{bmatrix} K\left(\mathbf{A}, \mathbf{A}^T\right)^T \\ \mathbf{e}^T \end{bmatrix}\boldsymbol{\alpha} + c_1\begin{bmatrix} \boldsymbol{\omega}_1 \\ b_1 \end{bmatrix} = 0. \end{aligned} \tag{20}$$

Let $\mathbf{H} = [K(\mathbf{A}, \mathbf{A}^T)\mathbf{e}]$ and $\mathbf{u}_1 = [\boldsymbol{\omega}_1^T b_1]^T$, and (20) can be rewritten as

$$-\mathbf{H}^T\mathbf{D}_1\mathbf{y} + \left(\mathbf{H}^T\mathbf{D}_1\mathbf{H} + c_1\mathbf{I}\right)\mathbf{u}_1 + \mathbf{H}^T\boldsymbol{\alpha} = 0. \tag{21}$$

where $\mathbf{I}$ is an identity matrix with appropriate dimension. From (21), we get

$$\mathbf{u}_1 = \left(\mathbf{H}^T\mathbf{D}_1\mathbf{H} + c_1\mathbf{I}\right)^{-1}\mathbf{H}^T\left(\mathbf{D}_1\mathbf{y} - \boldsymbol{\alpha}\right). \tag{22}$$

From (15), (16), and (19), the following constraints can be obtained:

$$\mathbf{e}^T\boldsymbol{\alpha} \leq c_2\nu_1, \quad 0\mathbf{e} \leq \boldsymbol{\alpha} \leq c_2\mathbf{D}_2. \tag{23}$$

Substituting (22) into Lagrangian function L, we can get the dual formulation of (12)

$$\begin{aligned} \min_{\boldsymbol{\alpha}} \quad &\frac{1}{2}\boldsymbol{\alpha}^T\mathbf{H}\left(\mathbf{H}^T\mathbf{D}_1\mathbf{H} + c_1\mathbf{I}\right)^{-1}\mathbf{H}^T\boldsymbol{\alpha} + \mathbf{y}^T\boldsymbol{\alpha} \\ &- \mathbf{y}^T\mathbf{D}_1\mathbf{H}\left(\mathbf{H}^T\mathbf{D}_1\mathbf{H} + c_1\mathbf{I}\right)^{-1}\mathbf{H}^T\boldsymbol{\alpha} \\ \text{s.t.:} \quad &0\mathbf{e} \leq \boldsymbol{\alpha} \leq c_2\mathbf{D}_2, \quad \mathbf{e}^T\boldsymbol{\alpha} \leq c_2\nu_1. \end{aligned} \tag{24}$$

Similarly, the dual formulation of (13) can be derived as follows:

$$\begin{aligned} \min_{\boldsymbol{\eta}} \quad &\frac{1}{2}\boldsymbol{\eta}^T\mathbf{H}\left(\mathbf{H}^T\mathbf{D}_1\mathbf{H} + c_3\mathbf{I}\right)^{-1}\mathbf{H}^T\boldsymbol{\eta} \\ &+ \mathbf{y}^T\mathbf{D}_1\mathbf{H}\left(\mathbf{H}^T\mathbf{D}_1\mathbf{H} + c_3\mathbf{I}\right)^{-1}\mathbf{H}^T\boldsymbol{\eta} - \mathbf{y}^T\boldsymbol{\eta} \\ \textit{st:} \quad &0\mathbf{e} \leq \boldsymbol{\eta} \leq c_4\mathbf{D}_2, \quad \mathbf{e}^T\boldsymbol{\eta} \leq c_4\nu_2. \end{aligned} \tag{25}$$

To solve the above QPPs, the vectors $\boldsymbol{\omega}_1, b_1$ and $\boldsymbol{\omega}_2, b_2$ can be expressed by

$$\begin{bmatrix} \boldsymbol{\omega}_1 \\ b_1 \end{bmatrix} = \left(\mathbf{H}^T\mathbf{D}_1\mathbf{H} + c_1\mathbf{I}\right)^{-1}\mathbf{H}^T\left(\mathbf{D}_1\mathbf{y} - \boldsymbol{\alpha}\right), \tag{26}$$

and

$$\begin{bmatrix} \boldsymbol{\omega}_2 \\ b_2 \end{bmatrix} = \left(\mathbf{H}^T\mathbf{D}_1\mathbf{H} + c_3\mathbf{I}\right)^{-1}\mathbf{H}^T\left(\mathbf{D}_1\mathbf{y} + \boldsymbol{\eta}\right). \tag{27}$$

By substituting the above results into (3), the final regression function can be obtained.

2.3.2. Determination of Wavelets Transform Based Weighted Matrix $\mathbf{D}_1$ and a Coefficient Vector $\mathbf{D}_2$. The wavelet transform can be used to denoise the time series signal. Based on the work of Ingrid Daubechies, the Daubechies wavelets

are a family of orthogonal wavelets for a discrete wavelet transform. There is a scaling function (called father wavelet) for each wavelet type, which generates an orthogonal multiresolution analysis. Daubechies orthogonal wavelets $db1$ – $db10$ are commonly used.

The wavelet transform process includes three stages: decomposition, signal processing, and reconstruction. In each step of decomposition, the signal can be decomposed into two sets of signals: high frequency signal and low frequency signal. Suppose that there is a time series signal $\mathbf{S}$. After the first step of decomposition, it generates two signals: one is high frequency part $\mathbf{Sh}_1$ and another is low frequency part $\mathbf{Sl}_1$. Then, in the second step of decomposition, the low frequency signal $\mathbf{Sl}_1$ can be decomposed further into $\mathbf{Sh}_2$ and $\mathbf{Sl}_2$. After k steps of decomposition, $k+1$ groups of decomposed sequence $(\mathbf{Sh}_1, \mathbf{Sh}_2, \ldots, \mathbf{Sh}_k, \mathbf{Sl}_k)$ are obtained, where $\mathbf{Sl}_k$ represents the contour of the original signal $\mathbf{S}$ and $\mathbf{Sh}_1, \mathbf{Sh}_2, \ldots, \mathbf{Sh}_k$ represent the subtle fluctuations. The decomposition process of signal $\mathbf{S}$ is shown in Figure 1 and defined as follows:

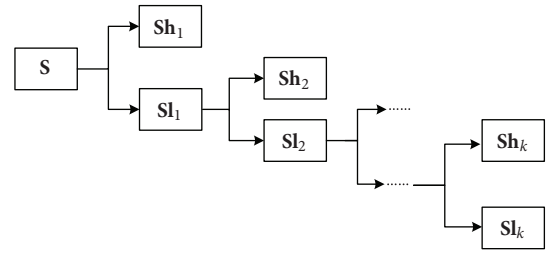

Figure 1: The process of decomposition.

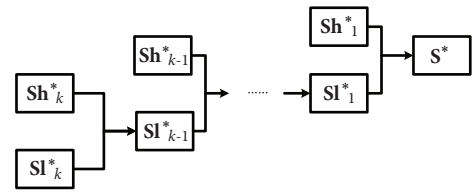

Figure 2: The process of reconstruction.

$$\mathbf{Sl}_k(n) = \sum_{m=1}^{l_{k-1}} \phi(m-2n)\,\mathbf{Sl}_{k-1}(m) \tag{28}$$

$$\mathbf{Sh}_k(n) = \sum_{m=1}^{l_{k-1}} \varphi(m-2n)\,\mathbf{Sl}_{k-1}(m) \tag{29}$$

where $\mathbf{Sl}_{k-1}$ with the length l_{k-1} is the signal to be decomposed, $\mathbf{Sl}_k$ and $\mathbf{Sh}_k$ are the results in the k-th step. $\phi(m-2n)$, and $\varphi(m-2n)$ are called scaling sequence (low pass filter) and wavelets sequence, respectively [24]. In this paper, $db2$ wavelet with the length of 4 is adopted. After wavelet transforming, appropriate signal processing can be carried out. In the stage of reconstruction, the processed high frequency signal $\mathbf{Sh}_k^*$ and low frequency signal $\mathbf{Sl}_k^*$ are reconstructed to generate the target signal $\mathbf{S}^*$. Let $\mathbf{P}$ and $\mathbf{Q}$ be the matrix with the order of $l_k \times l_{k-1}$, $\mathbf{P}_{n,m} = \phi(m-2n)$, and $\mathbf{Q}_{n,m} = \varphi(m-2n)$. The reconstruction process is shown in Figure 2. Therefore, (28) and (29) can be rewritten as follows:

$$\mathbf{Sl}_k(n) = \mathbf{P} \cdot \mathbf{Sl}_{k-1}(m) \tag{30}$$

$$\mathbf{Sh}_k(n) = \mathbf{Q} \cdot \mathbf{Sl}_{k-1}(m) \tag{31}$$

The signal $\mathbf{Sl}_{k-1}^*$ can be generated by reconstructing $\mathbf{Sl}_k^*$ and $\mathbf{Sh}_k^*$:

$$\mathbf{Sl}_{k-1}^*(m) = \mathbf{P}^{-1} \cdot \mathbf{Sl}_k^*(n) + \mathbf{Q}^{-1} \cdot \mathbf{Sh}_k^*(n) \tag{32}$$

If the output vector $\mathbf{S} = [S_1, S_2, \ldots, S_l]^T$ of a prediction model is a time sequence, then the wavelets transform can be used to denoise the output of the training samples. After the decomposition, signal processing, and reconstruction process, a denoising sequence $\mathbf{S}^* = [S_1^*, S_2^*, \ldots, S_l^*]^T$ can be obtained. The absolute difference vector $r_i = |S_i - S_i^*|$, $i = 1, 2, \ldots, l$, and $\mathbf{r} = [r_1, r_2, \ldots, r_l]^T$ between S and S^* denote the distance from the training samples to the denoising samples. In the WTWTSVR, a small, r_i, reflects a large weight on the distance between the estimated value and training value of the i-th sample, which can be defined as the following Gaussian function:

$$d_i = \exp\left(-\frac{r_i^2}{2\sigma^{*2}}\right), \quad i = 1, 2, \ldots, l, \tag{33}$$

where d_i denotes the weight coefficient and σ^* is the width of the Gaussian function. Therefore, the wavelets transform based weighted matrix $\mathbf{D}_1$ and the coefficient vector $\mathbf{D}_2$ can be determined by $\mathbf{D}_1 = \mathrm{diag}(d_1, d_2, \ldots, d_l)$ and $\mathbf{D}_2 = [d_1, d_2, \ldots, d_l]^T$.

2.3.3. Computational Complexity Analysis. The computation complexity of the proposed algorithm is mainly determined by the computations of a pair of QPPs and a pair of inverse matrices. If the number of the training samples is l, then the training complexity of dual QPPs is about $O(2l^3)$, while the training complexity of the traditional SVR is about $O(8l^3)$, which implies that the training speed of SVR is about four times the proposed algorithm. Also, a pair of inverse matrices with the size $(l+1) \times (l+1)$ in QPPs have the same computational cost $O(l^3)$. During the training process, it is a good way to cache the pair of inverse matrices with some memory cost in order to avoid repeated computations. In addition, the proposed algorithm contains the wavelet transform weighted matrix and $db2$ wavelet with length of 4 is used in this paper. Then, the complexity of wavelet transform is less than $8l$. By comparing with the computations of QPPs and inverse matrix, the complexity of computing the wavelet matrix can be ignored. Therefore, the computation complexity of the proposed algorithm is about $O(3l^3)$.

3. Establishment of Static Control Model

The end-point carbon content (denoted as C) and the temperature (denoted as T) are main factors to test the quality of steelmaking. The ultimate goal of steelmaking is to control

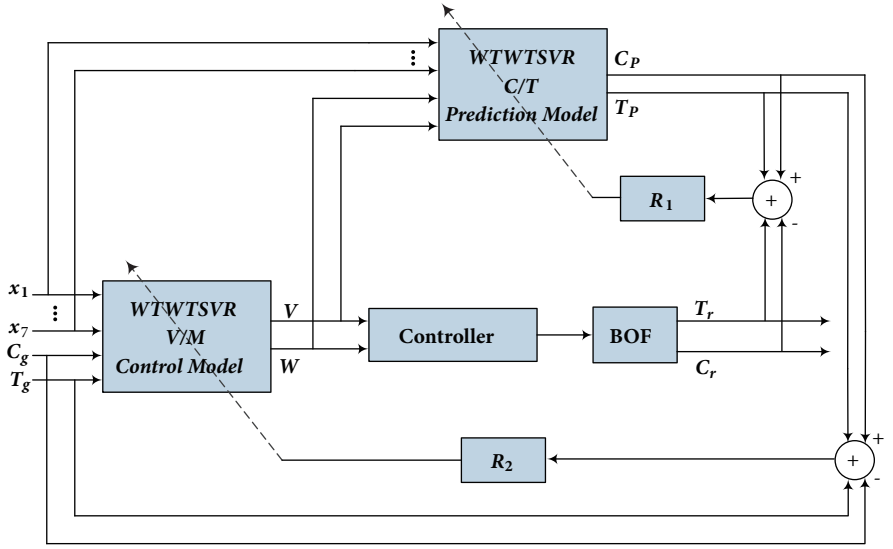

Figure 3: Structure of proposed BOF control model.

C and T to a satisfied region. BOF steelmaking is a complex physicochemical process, so its mathematical model is very difficult to establish. Therefore, the intelligent method such as TSVR can be used to approximate the BOF model. From the collected samples, it is easy to see that the samples are listed as a time sequence, which means they can be seen as a time sequence signal. Hence, the proposed WTWTSVR algorithm is appropriate to establish a model for BOF steelmaking.

In this section, a novel static control model for BOF is established based on WTWTSVR algorithm. According to the initial conditions of the hot metal and the desired end-point carbon content (denoted as C_g) and the temperature (denoted as T_g), the relative oxygen blowing volume (denoted as V) and the weight of auxiliary raw material (denoted as W) can be calculated by the proposed model. Figure 3 shows the structure of the proposed BOF control model, which is composed of a prediction model for carbon content and temperature (C/T prediction model), a control model for oxygen blowing volume and the weight of auxiliary raw materials (V/W control model), two parameter regulating units (R_1 and R_2), and a controller and a basic oxygen furnace in any plant. Firstly, the WTWTSVR C/T prediction model should be established by using the historic BOF samples, which consists of two individual models (C_model and T_model). C_model represents the prediction model of the end-point carbon content and T_model represents the prediction of the end-point temperature. The inputs of two models both include the initial conditions of the hot metal, and the outputs of them are C and T, respectively. The parameters of the prediction models can be regulated by R_1 to obtain the optimized models. Secondly, the WTWTSVR V/W control model should be established based on the proposed prediction models, and the oxygen blowing volume can be calculated by V_model and the weight of auxiliary raw materials can be determined by W_model. The inputs of the control models both include the initial conditions of the hot metal, the desired end-point carbon content C_g), and the end-point temperature T_g. The outputs of them are V and W, respectively. The parameters of the control models can be regulated by R_2. After the regulation of R_1 and R_2, the static control model can be established. For any future hot metal, the static control model can be used to calculate V and W by the collected initial conditions and C_g and T_g. Then, the calculated values of V and W will be sent to the controller. Finally, the relative BOF system is controlled by the controller to reach the satisfactory end-point region.

3.1. Establishment of WTWTSVR C/T Prediction Model. To realize the static BOF control, an accurate prediction model of BOF should be designed firstly. The end-point prediction model is the foundation of the control model. By collecting the previous BOF samples, the abnormal samples must be discarded, which may contain the wrong information of BOF. Through the mechanism analysis of BOF, the influence factors on the end-point information are mainly determined by the initial conditions of hot metal, which means the influence factors are taken as the independent input variables of the prediction models. The relative input variables are listed in Table 1. Note that the input variable x_9 denotes the sum of the weight of all types of auxiliary materials, which are including the light burned dolomite, the dolomite stone, the lime ore and scrap, etc. It has a guiding significance for real production, and the proportion of the components can be determined by the experience of the user. The output variable of the model is the end-point carbon content C or the end-point temperature T.

According to the prepared samples of BOF and WTWTSVR algorithm, the regression function $f_{C/T}(x)$ can be given by

$$f_{C/T}(\mathbf{x}) = \frac{1}{2}K\left(\mathbf{x}^T, \mathbf{A}^T\right)\left(\boldsymbol{\omega}_1 + \boldsymbol{\omega}_2\right)^T + \frac{1}{2}\left(b_1 + b_2\right) \quad (34)$$

where $f_{C/T}(\mathbf{x})$ denotes the estimation function of C_model or T_model and $\mathbf{x} = [x_1, x_2, \ldots, x_9]^T$.

Table 1: Independent input variables of prediction models.

Name of input variable	Symbol	Units	Name of input variable	Symbol	Units
Initial carbon content	x_1	%	Sulphur content	x_6	%
Initial temperature	x_2	˚C	Phosphorus content	x_7	%
Charged hot metal	x_3	*tons*	Oxygen blowing volume	$x_8\ (V)$	Nm^3
Silicon content	x_4	%	Total weight of auxiliary raw materials	$x_9\ (W)$	*tons*
Manganese content	x_5	%			

Out of the historical data collected from one BOF of 260 *tons* in some steel plant in China, 220 samples have been selected and prepared. In order to establish the WTWTSVR prediction models, the first 170 samples are taken as the training data and 50 other samples are taken as the test data to verify the accuracy of the proposed models. In the regulating unit R_1, the appropriate model parameters ($c_1, c_2, c_3, c_4, \nu_1, \nu_2$, and σ_1, σ_1^*) are regulated manually, and then the C_model and T_model can be established. In summary, the process of the modelling can be described as follows.

Step 1. Initialize the parameters of the WTWTSVR prediction model, and normalize the prepared 170 training samples from its original range to the range $[-1\ \ 1]$ by *mapminmax* function in Matlab.

Step 2. Denoise the end-point carbon content $\mathbf{C} = [C_1, C_2, \ldots, C_l]^T$ or temperature $\mathbf{T} = [T_1, T_2, \ldots, T_l]^T$ in the training samples by using the wavelet transform described in the previous section. Then, the denoised samples $\mathbf{C}^* = [C_1^*, C_2^*, \ldots, C_l^*]^T$ and $\mathbf{T}^* = [T_1^*, T_2^*, \ldots, T_l^*]^T$ can be obtained.

Step 3. By selecting the appropriate parameter σ_1^* in (33), determine the wavelets transform based weighted matrix $\mathbf{D}_1$ and the coefficient vector $\mathbf{D}_2$.

Step 4. Select appropriate values of $c_1, c_2, c_3, c_4, \nu_1, \nu_2$ and σ_1 in the regulating unit R_1.

Step 5. Solve the optimization problems in (24) and (25) by *quadprog* function in Matlab and return the optimal vector $\boldsymbol{\alpha}$ or $\boldsymbol{\eta}$.

Step 6. Calculate the vectors $\boldsymbol{\omega}_1, b_1$ and $\boldsymbol{\omega}_2, b_2$ by (26) and (27).

Step 7. Substitute the parameters in Step 5 into (3) to obtain the function $f_{C/T}(\mathbf{x})$.

Step 8. Substitute the training samples into (34) to calculate the relative criteria of the model, which will be described in details later.

Step 9. If the relative criteria are satisfactory, then the C_model or T_model is established. Otherwise, return to Steps from 4 to 8.

3.2. Establishment of WTWTSVR V/W Control Model. Once the WTWTSVR C/T prediction models are established, the WTWTSVR V/W control models are ready to build. In order to control the end-point carbon content and temperature to the satisfactory region for any future hot metal, the relative oxygen blowing volume V and the total weight of auxiliary raw materials W should be calculated based on V/W control models, respectively. Through the mechanism analysis, the influence factors on V and W are mainly determined by the initial conditions of hot metal, and the desired conditions of the steel are also considered as the the influence factors. Then, the independent input variables of the control models are listed in Table 2, where the input variables x_1-x_7 are the same as the C/T prediction model and other two input variables are the desired carbon content C_g and desired temperature T_g, respectively. The output variable of the control model is V or W defined above.

Similar to (34), the regression function $f_{V/W}(\mathbf{x})$ can be written as

$$f_{V/W}(\mathbf{x}) = \frac{1}{2}K\left(\mathbf{x}^T, \mathbf{A}^T\right)\left(\boldsymbol{\omega}_3 + \boldsymbol{\omega}_4\right)^T + \frac{1}{2}\left(b_3 + b_4\right) \quad (35)$$

where $f_{V/W}(\mathbf{x})$ denotes the estimation function of V_model or W_model and $\mathbf{x} = [x_1, x_2, \ldots, x_9]^T$.

In order to establish the WTWTSVR control models, the training samples and the test samples are the same as that of the prediction models. The regulating unit R_2 is used to regulate the appropriate model parameters ($c_5, c_6, c_7, c_8, \nu_3, \nu_4$ and σ_2, σ_2^*) manually; then the V_model and W_model can be established. In summary, the process of the modelling can be described as follows.

Steps 1–7. Similar to those in the section of establishing the prediction models except for the input variables listed in Table 2 and the output variable being the oxygen blowing volume $\mathbf{V} = [V_1, V_2, \ldots, V_l]^T$ or the total weight of auxiliary materials $\mathbf{W} = [W_1, W_2, \ldots, W_l]^T$. Also, select appropriate values of $c_5, c_6, c_7, c_8, \nu_3, \nu_4$ and σ_2 in the regulating unit R_2; then the function $f_{V/W}(\mathbf{x})$ is obtained.

Step 8. Substitute the training samples into (35) to calculate the relative predicted values $\widehat{V}$ and $\widehat{W}$ of V and W respectively.

Step 9. $\widehat{V}$ and $\widehat{W}$ are combined with the input variables $x_1 - x_7$ in Table 1 to obtain 50 new input samples. Then, substituting them into the C_model and T_model, 50 predicted values $\widehat{C}$ and $\widehat{T}$ can be obtained. Finally, calculate the differences between the desired values C_g, T_g and the predicted values $\widehat{C}, \widehat{T}$. Also, other relative criteria of the model should be determined.

Table 2: Independent input variables of control models.

Name of input variable	Symbol	Units	Name of input variable	Symbol	Units
Initial carbon content	x_1	%	Sulphur content	x_6	%
Initial temperature	x_2	°C	Phosphorus content	x_7	%
Charged hot metal	x_3	*tons*	Desired carbon content	x_8 (C_g)	Nm^3
Silicon content	x_4	%	Desired temperature	x_9 (T_g)	*tons*
Manganese content	x_5	%			

Step 10. If the obtained criteria are satisfactory, then the V_model or W_model is established. Otherwise, return to Steps from 4 to 9.

4. Results and Discussion

In order to verify the performances of WTWTSVR algorithm and proposed models, the artificial functions and practical datasets are adopted, respectively. All experiments are carried out in Matlab R2011b on Windows 7 running on a PC with Intel (R) Core (TM) i7-4510U CPU 2.60GHz with 8GB of RAM.

The evaluation criteria are specified to evaluate the performance of the proposed method. Assume that the total number of testing samples is n, y_i is the actual value at the sample point x_i, $\widehat{y}_i$ is the estimated value of y_i, and $\overline{y}_i = (\sum_{i=1}^{n} y_i)/n$ is the mean value of $y_1, y_2, \ldots, y_n$. Therefore, the following criteria can be defined:

$$RMSE = \sqrt{\frac{1}{n}\sum_{i=1}^{n}(y_i - \widehat{y}_i)^2}, \tag{36}$$

$$MAE = \frac{1}{n}\sum_{i=1}^{n}\left|y_i - \widehat{y}_i\right|, \tag{37}$$

$$\frac{SSE}{SST} = \frac{\sum_{i=1}^{n}(y_i - \widehat{y}_i)^2}{\sum_{i=1}^{n}(y_i - \overline{y}_i)^2}, \tag{38}$$

$$\frac{SSR}{SST} = \frac{\sum_{i=1}^{n}(\widehat{y}_i - \overline{y}_i)^2}{\sum_{i=1}^{n}(y_i - \overline{y}_i)^2}, \tag{39}$$

$$HR = \frac{Number\ of\ \left|y_i - \widehat{y}_i\right| < error\ bound}{n} \times 100\%, \tag{40}$$

In the above equations, *RMSE* denotes the root mean squared error, *MAE* denotes the mean absolute error, and *SSE*, *SST*, and *SSR* represent the sum of the squared deviation between any two of $y_i, \widehat{y}_i, \overline{y}_i$, respectively. Normally, a smaller value of *SSE*/*SST* reflects that the model has a better performance. The decrease in *SSE*/*SST* reflects the increase in *SSR*/*SST*. However, if the value of *SSE*/*SST* is extremely small, it will cause the overfitting problem of the regressor. An important criteria for evaluating the performance of the BOF model is hit rate (*HR*) calculated by (40), which is defined as the ratio of the number of the satisfactory samples over the total number of samples. For any sample in the dataset, if the absolute error between the estimated value and actual value is smaller than a certain error bound, then the results of the sample hit the end point. A large number of hit rate indicate a better performance of the BOF model. Generally, a hit rate of 90% for C or T is a satisfactory value in the real steel plants.

4.1. Performance Test of WTWTSVR. In this section, the artificial function named Sinc function is used to test the regression performance of the proposed WTWTSVR method, which can be defined as $y = \sin x/x,\ x \in [-4\pi, 4\pi]$.

In order to evaluate the proposed method effectively, the training samples are polluted by four types of noises, which include the Gaussian noises with zero means and the uniformly distributed noises. For the train samples $(x_i, y_i),\ i = 1, 2, \ldots, l$, we have

$$y_i = \frac{\sin x_i}{x_i} + \theta_i, \quad x \sim U[-4\pi, 4\pi],\ \theta_i \sim N\left(0, 0.1^2\right), \tag{41}$$

$$y_i = \frac{\sin x_i}{x_i} + \theta_i, \quad x \sim U[-4\pi, 4\pi],\ \theta_i \sim N\left(0, 0.2^2\right), \tag{42}$$

$$y_i = \frac{\sin x_i}{x_i} + \theta_i, \quad x \sim U[-4\pi, 4\pi],\ \theta_i \sim U[0, 0.1], \tag{43}$$

$$y_i = \frac{\sin x_i}{x_i} + \theta_i, \quad x \sim U[-4\pi, 4\pi],\ \theta_i \sim U[0, 0.2], \tag{44}$$

where $U[m, n]$ and $N(p, q^2)$ denote the uniformly random variable in $[m, n]$ and the Gaussian variable with the mean p and variance q^2, respectively. For all regressions of the above four Sinc functions, 252 training samples and 500 test samples are selected. Note that the test samples are uniformly sampled from the Sinc functions without any noise. For all algorithms in this paper, the following sets of parameters are explored: the penalty coefficient c is searched from the set $\{i/1000, i/100, i/10 \mid i = 1, 2, \ldots, 10\}$. The tube regulation coefficient v is selected from the set $\{1, 2, \ldots, 10\}$. The wavelet coefficient σ and kernel parameter σ^* are both searched over the range $\{i/1000, i/100, i/10, i \mid i = 1, 2, \ldots, 10\}$. In order to reduce the number of combinations in the parameter search, the following relations are chosen: $c_1 = c_3$, $c_2 = c_4$, and $v_1 = v_2$.

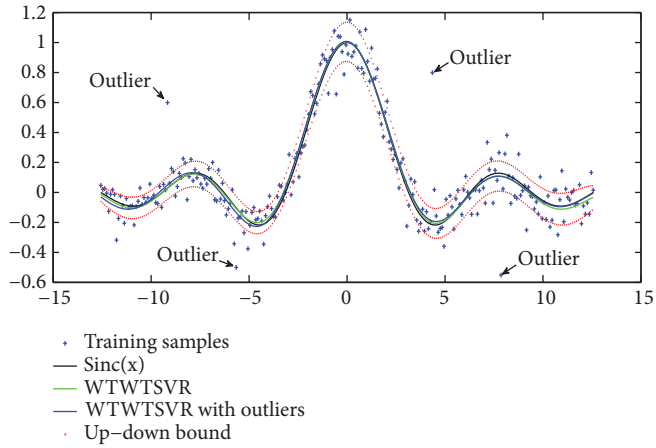

Figure 4: Performance of WTWTSVR on Sinc function with and without outliers.

Firstly, the choice of kernel function should be considered, RBF kernel is an effective and frequently used kernel function in TSVR research papers. Also, the performance of RBF has been evaluated by comparing with other three existing kernel functions (listed in Table 3), and the results are shown in Table 4. It is easy to see that the RBF kernel achieves the optimal results. Then, the average results of the proposed methods and other four existing methods (TSVR [15], ν-TSVR [17], KNNWTSVR [19] and Asy ν-TSVR [20]) with 10 independent runs are shown in Table 5, where Type A, B, C and D denote four different types of noises (41)-(44). Obviously, the results of Table 5 show that the proposed method achieves the optimal result of *SSE*. Also, the proposed method achieves the smallest *SSE*/*SST* results in four regressions of Sinc functions, which are 0.0029, 0.0124, 0.0231 and 0.0903. Especially, the obvious performances are enhanced in Type A and B. The *SSR*/*SST* of the proposed method takes the first position in Type B, the second position in Type A and C, and the third position in Type D. From the aspect of training time, it can be seen that the proposed method achieves the optimal result in Type B. In Type A, C and D, the training time of the proposed method is faster than that of TSVR and KNNWTSVR, and close to ν-Type and Asy ν-Type. It verifies that the computational complexity of wavelet transform weighting scheme is lower than KNN weighting scheme. For the effect of outliers, we have verified the performance of the proposed method on the Sinc function with Type A noise. Figure 4 shows that the prediction performance of the proposed method is satisfied against the outliers, as shown in the blue line, and the results of *SSE*, *SSE*/*SST* and *SSR*/*SST* achieve 0.1911, 0.0036 and 1.0372, respectively. By comparing with the results in Table 5, it can be concluded that the overall performance of the proposed method with outliers is still better than TSVR, v-TSVR and KNNWTSVR. Therefore, it can be concluded that the overall regression performance of the proposed method is optimal.

4.2. Verification of the Proposed BOF Models. In order to verify the effectiveness of the proposed model, 240 heats samples for low carbon steel of 260*tons* BOF were collected from some steel plant in China. Firstly, the preprocessing of the samples should be carried out. The abnormal samples with the unexpected information must be removed, which exceeds the actual range of the signals. It may be caused by the wrong sampling operation. Then, 220 qualified samples are obtained. The next step is to analyze the information of the qualified samples. The end-point carbon content and temperature are mainly determined by the initial conditions of the iron melt, the total blowing oxygen volume and the weight of material additions. Therefore, the unrelated information should be deleted, such as the heat number, the date of the steelmaking and so on. According to the information of Tables 1 and 2, the datasets for the relative prediction and control models can be well prepared. After that, the proposed models are ready to be established. More details of the model have been described in Section 3. The proposed control model consists of two prediction models (C_model and T_model) and two control models (V_model and W_model). For each individual model, there are 8 parameters that need to be regulated to achieve the satisfactory results. The regulation processes are related to the units R_1 and R_2 in Figure 3. First of all, the prediction models need to be established. In order to meet the requirements of the real production, the prediction errors bound with 0.005% for C_model and 10°C for T_model are selected. Similarly, the control errors bound with 800 Nm^3 for V_model and 5.5 *tons* for W_model are selected. The accuracy of each model can be reflected by the hit rate with its relative error bound, and a hit rate of 90% within each individual error bound is a satisfied result.

Table 3: Type and functions of four existing kernel functions.

Kernel Type	Function
Radial Basis Function Kernel (RBF)	$K(\mathbf{x}, \mathbf{x}_i) = \exp\left(-\frac{\|\mathbf{x}-\mathbf{x}_i\|^2}{2\sigma^2}\right)$
Rational Quadratic Kernel (RQ)	$K(\mathbf{x}, \mathbf{x}_i) = 1 - \frac{\|\mathbf{x}-\mathbf{x}_i\|^2}{\left(\|\mathbf{x}-\mathbf{x}_i\|^2 + \sigma\right)}$
Multiquadric Kernel	$K(\mathbf{x}, \mathbf{x}_i) = \left(\|\mathbf{x}-\mathbf{x}_i\|^2 + \sigma^2\right)^{0.5}$
Log Kernel	$K(\mathbf{x}, \mathbf{x}_i) = -\log\left(1 + \|\mathbf{x}-\mathbf{x}_i\|^{\sigma}\right)$

Table 4: . Comparisons of WTWTSVR on Sinc functions with different kernel functions.

Noise	Kernel Type	*SSE*	*SSE/SST*	*SSR/SST*
Type A	RBF	**0.1577±0.0099**	**0.0029±0.0018**	**0.9972±0.0264**
	RQ	0.1982±0.0621	0.0037±0.0012	1.0157±0.0297
	Multiquadric	0.2884±0.0762	0.0054±0.0014	0.9911±0.0345
	Log	0.4706±0.1346	0.0088±0.0025	1.0115±0.0306
Type B	RBF	**0.6659±0.2456**	**0.0124±0.0046**	**1.0161±0.0564**
	RQ	1.1662±0.3175	0.0217±0.0059	0.9834±0.0385
	Multiquadric	1.1101±0.5028	0.0206±0.0093	1.0030±0.0867
	Log	1.8157±0.6026	0.0338±0.0112	1.0366±0.0802
Type C	RBF	**1.2425±0.1444**	**0.0231±0.0027**	**1.0228±0.0153**
	RQ	3.5697±1.5023	0.0664±0.0279	1.0421±0.1584
	Multiquadric	3.6438±1.4810	0.0678±0.0275	1.0494±0.0641
	Log	6.9962±2.2691	0.1301±0.0422	1.1208±0.1682
Type D	RBF	**4.8557±0.4009**	**0.0903±0.0075**	**1.0768±0.0283**
	RQ	6.1541±1.8766	0.1144±0.0349	1.0829±0.1923
	Multiquadric	5.6597±2.4049	0.1052±0.0447	1.1015±0.1908
	Log	14.9196±3.4583	0.2774±0.0643	1.3255±0.2159

Table 5: Comparisons of four regression methods on Sinc functions with different noises.

Noise	Regressor	*SSE*	*SSE/SST*	*SSR/SST*	Time, *s*
Type A	WTWTSVR	**0.1577±0.0099**	**0.0029±0.0018**	0.9972±0.0264	1.7997
	TSVR	0.2316±0.1288	0.0043±0.0024	1.0050±0.0308	2.3815
	v-TSVR	0.4143±0.1261	0.0077±0.0023	0.9501±0.0270	1.7397
	Asy *v*-TSVR	0.1742±0.1001	0.0032±0.0019	1.0021±0.0279	1.7866
	KNNWTSVR	0.2044±0.0383	0.0038±0.0007	1.0177±0.0202	3.5104
Type B	WTWTSVR	**0.6659±0.2456**	**0.0124±0.0046**	**1.0161±0.0564**	**1.8053**
	TSVR	0.8652±0.3006	0.0161±0.0056	1.0185±0.0615	2.3296
	v-TSVR	0.8816±0.3937	0.0164±0.0073	0.9631±0.0548	1.8582
	Asy *v*-TSVR	0.7900±0.2588	0.0147±0.0048	1.0168±0.0599	1.8450
	KNNWTSVR	0.6891±0.2571	0.0128±0.0048	0.9679±0.0392	3.6175
Type C	WTWTSVR	**1.2425±0.1444**	**0.0231±0.0027**	1.0228±0.0153	1.8010
	TSVR	1.2505±0.0650	0.0233±0.0012	1.0217±0.0091	2.3054
	v-TSVR	1.5351±0.1172	0.0285±0.0022	0.9750±0.0111	1.7888
	Asy *v*-TSVR	1.2464±0.0934	0.0232±0.0017	1.0256±0.0125	1.6888
	KNNWTSVR	2.2027±0.7245	0.0410±0.0135	1.0148±0.1556	4.1230
Type D	WTWTSVR	**4.8557±0.4009**	**0.0903±0.0075**	1.0768±0.0283	1.7803
	TSVR	5.0090±0.2172	0.0931±0.0040	1.0890±0.0131	2.2556
	v-TSVR	5.2580±0.2935	0.0978±0.0055	1.0386±0.0125	1.7578
	Asy *v*-TSVR	4.9659±0.2925	0.0923±0.0054	1.0889±0.0128	1.7441
	KNNWTSVR	4.9751±1.3262	0.0925±0.0274	1.0262±0.1538	4.4397

Also, an end-point double hit rate (*DHR*) of the prediction model is another important criterion for the real production, which means the hit rates of end-point carbon content and temperature are both hit for the same sample. Hence, 170 samples are used to train the prediction and control models, and 50 samples are adopted to test the accuracy of the models. For each run of the relative modelling, the results are returned to the user with the information of the evaluation criteria. It shows the accuracy and fitness of the models with the specific parameters. Smaller values of *RMSE*, *MAE*, and *SSE*/*SST* and larger values of *SSR*/*SST* and hit rate are preferred, which means the model has a better generalization and higher accuracy. The regulation units R_1 and R_2 are used to balance the above criteria by selecting the appropriate values of the parameters. Note that the principle of the parameter selection is satisfactory if the following results are obtained: $SSR/SST > 0.5$ and $HR > 85\%$ with the smallest *SSE*/*SST*. Especially, the double hit rate *DHR* should be greater than 80 or higher. For

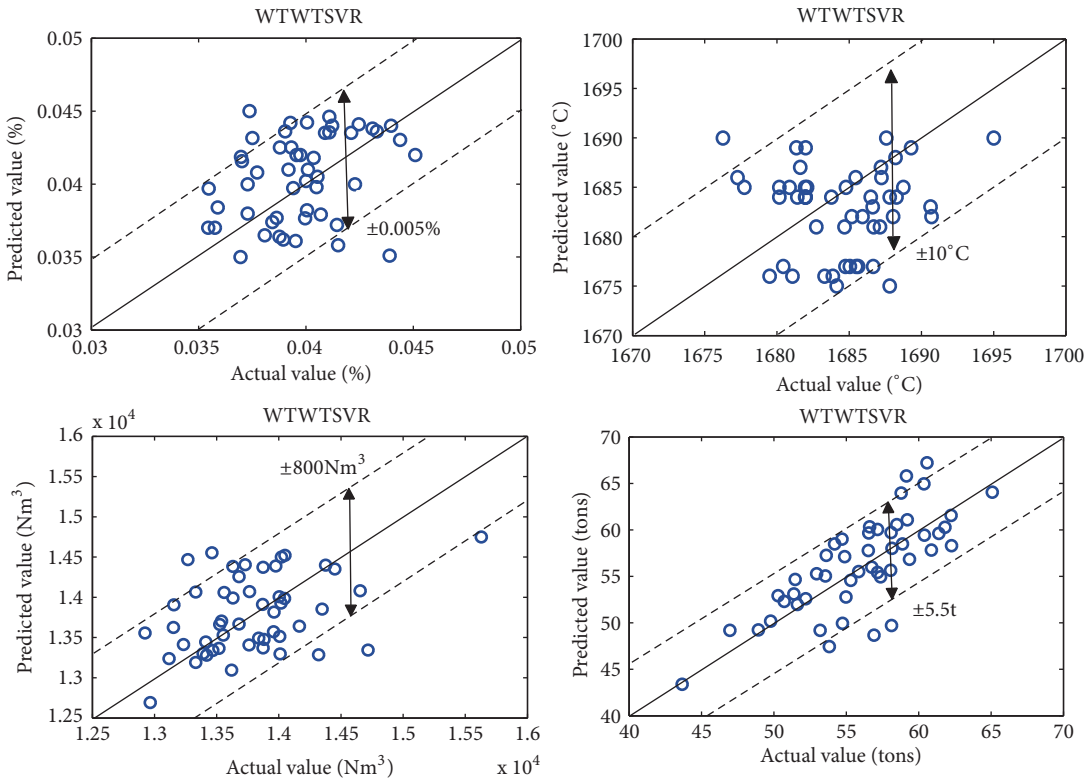

Figure 5: Performance of errors between predicted values and actual values with proposed static control model.

the collected samples, the parameters of WTWTSVR models are specified and shown in Table 6.

By using these parameters, the proposed BOF control model has been established. In order to evaluate the performance of the proposed method, more simulations of other existing regression methods with the samples are carried out, which are TSVR, v-TSVR, Asy v-TSVR, and KNNWTSVR, respectively. The comparison results of the carbon content prediction are listed in Table 7. From the results, it can be seen that the results of *RMSE*, *MAE*, and *SSE*/*SST* in the proposed method are 0.0023, 0.0026, and 1.1977, respectively. They are all smaller than those of other three existing methods, and the *SSR*/*SST* of 0.6930 is the highest result. The error performance and distribution of end-point carbon content between the predicted values and actual values are shown in Figures 5 and 6. It is clear that the proposed C_model can achieve the hit rate of 92%, which is better than other four methods. From above analysis, it illustrates that the proposed C_model has the best fitting behaviour for carbon content prediction.

Similarly, the performance comparisons of the temperature prediction are also listed in Table 7. From the results of Table 7, the best results of *RMSE* and *SSE*/*SST* and second best result of *MAE* of the proposed method are obtained. The results of *SSR*/*SST* is in the third position. Figures 5 and 6 show that the proposed T_model can achieve the hit rate of 96%, which is the optimal results by comparing with other methods. In addition, the double hit rate is also the key criterion in the real BOF applications; the proposed method can achieve a double hit rate of 90%, which is the best result, although the temperature hit rate of v-TSVR and KNNWTSVR method can also achieve 96%. However, their double hit rates only achieve 80% and 84%, respectively. In the real applications, a double hit rate of 90% is satisfactory. Therefore, the proposed model is more efficient to provide a reference for the real applications. Also, it meets the requirement of establishing the static control model.

Based on the prediction models, the control models (V_model and W_model) can be established by using the relative parameters in Table 6. The performance of the proposed V_model is shown in Figure 7. By comparing the proposed method with the existing methods, the comparison results of the oxygen blowing volume calculation are listed in Table 8, which shows that the results of *RMSE*, *MAE*, and *SSE*/*SST* in the proposed method are 371.3953, 411.7855, and 1.2713, respectively. They are all smaller than those of other four existing methods, and the *SSR*/*SST* of 1.0868 is in the fourth position. Figures 5 and 6 show that the predicted values of the proposed model agree well with the actual values of oxygen volume, and the proposed V_model has a best hit rate of 90%. It verifies that the proposed V_model has the best fitting behaviour for the calculation of oxygen blowing volume.

Similarly, the performance of the proposed W_model is shown in Figure 8, and the performance comparisons of the weight of the auxiliary materials are also listed in Table 8.

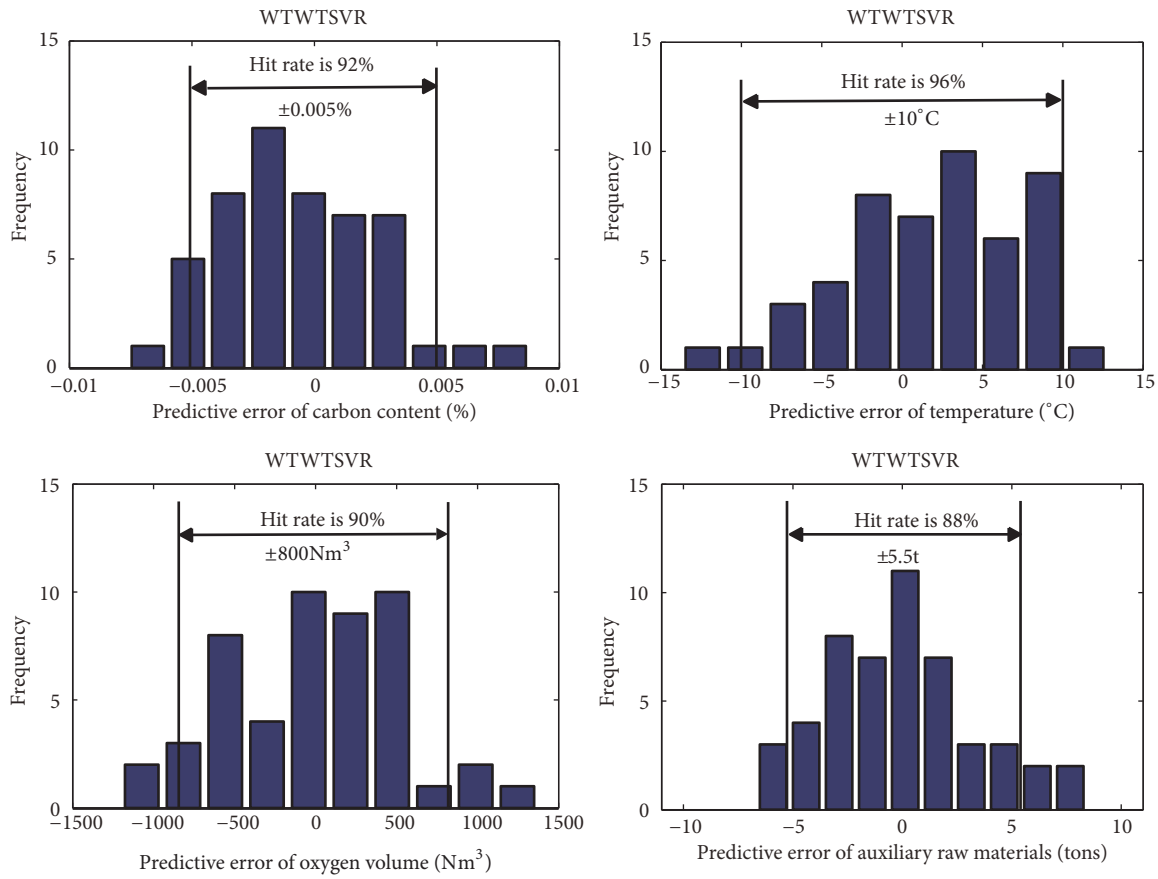

Figure 6: Performance of error distributions with proposed static control model.

Table 6: Specified parameters of prediction and control models.

Prediction Model	$c_1 = c_3$	$c_2 = c_4$	$v_1 = v_2$	σ_1	σ_1^*
C_model	0.005	0.02	3	0.005	1
T_model	0.002	0.05	5	0.04	0.3
Control Model	$c_5 = c_7$	$c_6 = c_8$	$v_3 = v_4$	σ_2	σ_2^*
V_model	0.002	0.01	2	0.2	3
W_model	0.001	0.02	1	0.5	5

Table 7: Performance comparisons of C/T prediction models with four methods.

Model	Criteria	WTWTSVR	TSVR	v-TSVR	Asy v-TSVR	KNNWTSVR
C_model (±0.005 %)	*RMSE*	**0.0023**	0.0026	0.0026	0.0026	0.0025
	MAE	**0.0026**	0.0031	0.0031	0.0031	0.0030
	SSE/*SST*	**1.1977**	1.6071	1.5675	1.5214	1.4680
	SSR/*SST*	**0.6930**	0.4616	0.3514	0.3835	0.3500
	HR,%	**92**	82	84	84	88
	Time, *s*	0.4523	0.2915	0.3706	0.3351	0.5352
T_model (±10 °C)	*RMSE*	**4.0210**	4.2070	4.3630	4.1013	4.0272
	MAE	4.7380	5.0363	5.1461	4.7970	4.7165
	SSE/*SST*	**1.7297**	1.8935	2.0365	1.7996	1.7351
	SSR/*SST*	0.7968	0.6653	0.7578	0.9141	0.8338
	HR,%	**96**	94	92	96	96
	Time, *s*	0.0977	0.1181	0.0861	0.0538	0.2393
	DHR,%	**90**	78	78	80	84

Table 8: Performance comparisons of V/W control models with four methods.

Model	Criteria	WTWTSVR	TSVR	v-TSVR	Asy v-TSVR	KNNWTSVR
V_model (±800 Nm^3)	*RMSE*	**371.3953**	383.0249	383.2387	399.8635	399.7568
	MAE	**411.7855**	416.3151	423.0260	427.0896	427.0415
	SSE/*SST*	**1.2713**	1.3522	1.3537	1.4737	1.4729
	SSR/*SST*	1.0868	1.1288	0.9691	0.9326	0.9319
	HR, %	**90**	86	84	86	86
	Time, *s*	0.6196	0.4397	0.5177	0.4883	0.7014
W_model (±5.5 *tons*)	*RMSE*	**2.4158**	2.8824	2.8431	3.6781	2.9077
	MAE	**2.7057**	3.1254	3.1632	3.9979	3.2588
	SSE/*SST*	**0.3791**	0.5398	0.5251	0.8789	0.5493
	SSR/*SST*	0.6505	0.5868	0.6739	0.4376	0.6725
	HR, %	**88**	86	80	80	84
	Time, *s*	0.1269	0.1230	0.0837	0.0609	0.2999
Hit rates	*HR* (C)	86	82	88	90	86
	HR (T)	92	94	94	80	94
	DHR	82	78	82	82	82

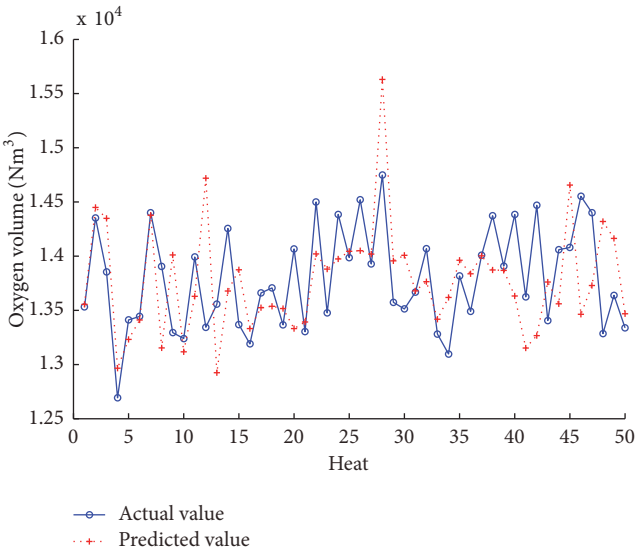

Figure 7: Performance of proposed V_model.

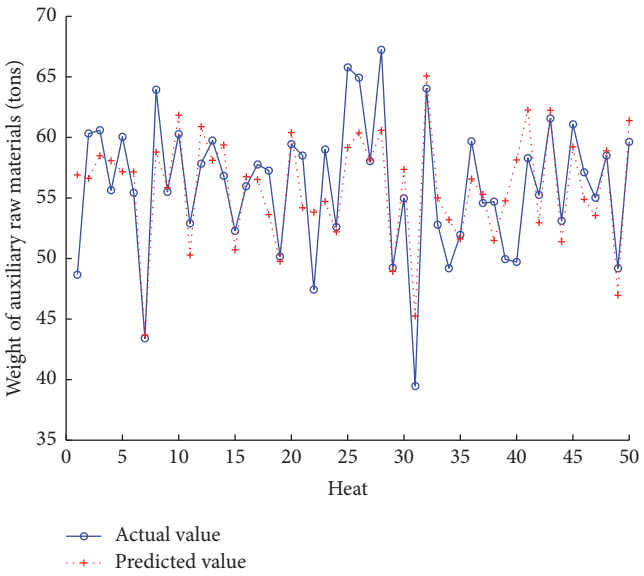

Figure 8: Performance of proposed W_model.

The proposed model achieves the best results of *RMSE*, *MAE*, and *SSE*/*SST*. Figures 5 and 6 show that the proposed method achieves the best hit rate of 88%. In addition, the training time of the proposed models is faster than that of KNNWTSVR method and slower than that of other three methods. It illustrates that the weighting scheme takes more time to obtain higher accuracy, and the performance of proposed weighting scheme is better than that of KNN weighting scheme for time sequence samples. For 50 test samples, there are 50 calculated values of V and W by V_model and W_model. Then, they are taken as the input variables into the proposed C_model and T_model to verify the end-point hit rate. From the results in Table 8, the proposed models can achieve a hit rate of 86% in C, 92% in T, and 82% in *DHR* is in the optimal result and the same as that of v-TSVR, Asy v-TSVR, and KNNWTSVR. In the real productions, *DHR* is paid more attention rather than the individual *HR* in C or T. Therefore, the proposed control models are verified to be able to guide the real production.

Based on above analysis, it can be concluded that the proposed static control model is effective and feasible; the hit rate can meet the requirements of the real productions for low carbon steel. For other types of steels, the proposed model is still suitable for use. Firstly, the specific samples of the heats should be obtained and preprocessed, and the analysis of the influence factors on the specific type of steel should be carried out to obtain the input variables of the model. The output variables are the same as the relative proposed models. Secondly, the end-point criteria should be specified, which is determined by the type of steel. Then, the parameters of the relative models can be regulated and determined to achieve the best criteria. Finally, the BOF control model for

the specific type of steel is established to guide the production in the plant.

BOF steelmaking is a complex physicochemical process; the proposed static control model can be established based on the real samples collected from the plant. However, there must be some undetected factors during the steelmaking process, which will affect the accuracy of the calculations of V and W. To solve this problem, the following strategies can be introduced: at the early stage of the oxygen blowing, the proposed control model is used to calculate the relative V and W and guide the BOF production. Then, the sublance technology is adopted at the late stage of oxygen blowing, because the physical and chemical reactions tend to be stable in this stage. Hence, the information of the melt liquid can be collected by the sublance. Therefore, another dynamic control model can be established with the sublance samples to achieve a higher end-point hit rate. For medium and small steel plants, the proposed static model is a suitable choice to reduce the consumption and save the cost.

Remark 3. Although this paper is mainly based on static control model, the prediction scheme is also compatible for other datasets over the globe. Especially, the proposed algorithm is competitive for the regression of time sequence datasets, such as the prediction of the blast furnace process and continuous casting process in the metallurgical industry.

5. Conclusion

In this paper, a WTWTSVR control model has been proposed. The new weighted matrix and the coefficient vector have been determined by the wavelet transform theory and added into the objective function of TSVR to improve the performance of the algorithm. The simulation results have shown that the proposed models are effective and feasible. The prediction error bound with 0.005% in C and 10°C in T can achieve a hit rate of 92% and 96%, respectively. In addition, the double hit rate of 90% is the best result by comparing with other three existing methods. The control error bound with 800 Nm^3 in V and 5.5 *tons* in W can achieve the hit rate of 90% and 88%, respectively. Therefore, the proposed method can provide a significant reference for real BOF applications. For the further work, on the basis of the proposed control model, a dynamic control model could be established to improve the end-point double hit rate of BOF up to 90% or higher.

Data Availability

The Excel data (Research Data.xls) used to support the findings of this study is included within the Supplementary Materials (available here).

Conflicts of Interest

The authors declare that they have no conflicts of interest.

Acknowledgments

This work was supported by Liaoning Province PhD Start-Up Fund (No. 201601291) and Liaoning Province Ministry of Education Scientific Study Project (No. 2017LNQN11).

Supplementary Materials

The supplementary material contains the Excel research data for our simulations. There are 220 numbers of preprocessed samples collected from one steel plant in China. Due to the limitations of confidentiality agreement, we cannot provide the name of the company. The samples include the historical information of hot metal, total oxygen volume, total weight of auxiliary raw materials, and end-point information. In the excel table, the variables from column A to K are mainly used to establish the static control model for BOF. Columns H, I, J, and K are the output variables for C_model, T_model, V_model, and W_model in the manuscript, respectively. The input variables of the relative models are listed in Tables 1 and 2. By following the design procedure of the manuscript, the proposed algorithm and other existing algorithms can be evaluated by using the provided research data. *(Supplementary Materials)*

References

[1] C. Blanco and M. Díaz, "Model of Mixed Control for Carbon and Silicon in a Steel Converter," *Transactions of the Iron & Steel Institute of Japan*, vol. 33, pp. 757–763, 2007.

[2] I. J. Cox, R. W. Lewis, R. S. Ransing, H. Laszczewski, and G. Berni, "Application of neural computing in basic oxygen steelmaking," *Journal of Materials Processing Technology*, vol. 120, no. 1-3, pp. 310–315, 2002.

[3] A. M. Bigeev and V. V. Baitman, "Adapting a mathematical model of the end of the blow of a converter heat to existing conditions in the oxygen-converter shop at the Magnitogorsk Metallurgical Combine," *Metallurgist*, vol. 50, no. 9-10, pp. 469–472, 2006.

[4] M. Brämming, B. Björkman, and C. Samuelsson, "BOF Process Control and Slopping Prediction Based on Multivariate Data Analysis," *Steel Research International*, vol. 87, no. 3, pp. 301–310, 2016.

[5] Z. Wang, F. Xie, B. Wang et al., "The control and prediction of end-point phosphorus content during BOF steelmaking process," *Steel Research International*, vol. 85, no. 4, pp. 599–606, 2014.

[6] M. Han and C. Liu, "Endpoint prediction model for basic oxygen furnace steel-making based on membrane algorithm evolving extreme learning machine," *Applied Soft Computing*, vol. 19, pp. 430–437, 2014.

[7] X. Wang, M. Han, and J. Wang, "Applying input variables selection technique on input weighted support vector machine modeling for BOF endpoint prediction," *Engineering Applications of Artificial Intelligence*, vol. 23, no. 6, pp. 1012–1018, 2010.

[8] M. Han and Z. Cao, "An improved case-based reasoning method and its application in endpoint prediction of basic oxygen furnace," *Neurocomputing*, vol. 149, pp. 1245–1252, 2015.

[9] L. X. Kong, P. D. Hodgson, and D. C. Collinson, "Modelling the effect of carbon content on hot strength of steels using a

modified artificial neural network," *ISIJ International*, vol. 38, no. 10, pp. 1121–1129, 1998.

[10] A. M. F. Fileti, T. A. Pacianotto, and A. P. Cunha, "Neural modeling helps the BOS process to achieve aimed end-point conditions in liquid steel," *Engineering Applications of Artificial Intelligence*, vol. 19, no. 1, pp. 9–17, 2006.

[11] S. M. Xie, J. Tao, and T. Y. Chai, "BOF steelmaking endpoint control based on neural network," *Control Theory Applications*, vol. 20, no. 6, pp. 903–907, 2003.

[12] J. Jiménez, J. Mochón, J. S. de Ayala, and F. Obeso, "Blast furnace hot metal temperature prediction through neural networks-based models," *ISIJ International*, vol. 44, no. 3, pp. 573–580, 2004.

[13] C. Kubat, H. Taşkin, R. Artir, and A. Yilmaz, "Bofy-fuzzy logic control for the basic oxygen furnace (BOF)," *Robotics and Autonomous Systems*, vol. 49, no. 3-4, pp. 193–205, 2004.

[14] Jayadeva, R. Khemchandani, and S. Chandra, "Twin support vector machines for pattern classification," *IEEE Transactions on Pattern Analysis and Machine Intelligence*, vol. 29, no. 5, pp. 905–910, 2007.

[15] X. Peng, "TSVR: an efficient Twin Support Vector Machine for regression," *Neural Networks*, vol. 23, no. 3, pp. 365–372, 2010.

[16] D. Gupta, "Training primal K-nearest neighbor based weighted twin support vector regression via unconstrained convex minimization," *Applied Intelligence*, vol. 47, no. 3, pp. 962–991, 2017.

[17] R. Rastogi, P. Anand, and S. Chandra, "A ν-twin support vector machine based regression with automatic accuracy control," *Applied Intelligence*, vol. 46, pp. 1–14, 2016.

[18] M. Tanveer, K. Shubham, M. Aldhaifallah, and K. S. Nisar, "An efficient implicit regularized Lagrangian twin support vector regression," *Applied Intelligence*, vol. 44, no. 4, pp. 831–848, 2016.

[19] Y. Xu and L. Wang, "K-nearest neighbor-based weighted twin support vector regression," *Applied Intelligence*, vol. 41, no. 1, pp. 299–309, 2014.

[20] Y. Xu, X. Li, X. Pan, and Z. Yang, "Asymmetric v-twin support vector regression," *Neural Computing and Applications*, vol. no. 2, pp. 1–16, 2017.

[21] N. Parastalooi, A. Amiri, and P. Aliheidari, "Modified twin support vector regression," *Neurocomputing*, vol. 211, pp. 84–97, 2016.

[22] Y.-F. Ye, L. Bai, X.-Y. Hua, Y.-H. Shao, Z. Wang, and N.-Y. Deng, "Weighted Lagrange ε-twin support vector regression," *Neurocomputing*, vol. 197, pp. 53–68, 2016.

[23] C. Gao, M. Shen, and L. Wang, "End-point Prediction of BOF Steelmaking Based on Wavelet Transform Based Weighted TSVR," in *Proceedings of the 2018 37th Chinese Control Conference (CCC)*, pp. 3200–3204, Wuhan, July 2018.

[24] J. Shen and G. Strang, "Asymptotics of Daubechies filters, scaling functions, and wavelets," *Applied and Computational Harmonic Analysis* , vol. 5, no. 3, pp. 312–331, 1998.